



## Towards improved modeling of steel-concrete composite wall elements

Frank J. Vecchio\*, Ian McQuade

University of Toronto, Civil Engineering Department, 35 St. George Street, Toronto, Canada, M5S 1A4

### ARTICLE INFO

#### Article history:

Received 28 January 2011

Received in revised form 1 April 2011

Accepted 2 April 2011

### ABSTRACT

The Disturbed Stress Field Model, a smeared rotating crack model for reinforced concrete based on the Modified Compression Field Theory, is adapted to the analysis of double-skin steel-concrete wall elements. The computational model is then incorporated into a two-dimensional nonlinear finite element analysis algorithm. Verification studies are undertaken by modeling various test specimens, including panel elements subject to uniaxial compression, panel elements subjected to in-plane shear, and wall specimens subjected to reversed cyclic lateral displacements. In all cases, the analysis model is found to provide accurate calculations of structural load capacities, pre- and post-peak displacement responses, post-peak ductility, chronology of damage, and ultimate failure mode. Minor deficiencies are found in regards to the accurate portrayal of faceplate buckling and the effects of interfacial slip between the faceplates and the concrete. Other aspects of the modeling procedure that are in need of further research and development are also identified and discussed.

© 2011 Elsevier B.V. All rights reserved.

### 1. Introduction

Steel-concrete (SC) composite wall elements generally consist of a thick concrete core section integral with thin steel faceplates. Typically the element contains no conventional in-plane reinforcement (i.e., no horizontal or vertical rebar) and no conventional shear reinforcement (i.e., no stirrups or T-headed bars). The steel skin plates are connected to the core with regularly spaced stud anchors. In some cases, cross tie-bars connecting the two steel faceplates are used, thus also functioning as shear reinforcement.

SC elements offer several advantages relative to conventional reinforced concrete (RC) walls. In particular, they lend themselves to more efficient construction practices, allowing the steel shells to be prefabricated in manageable sized panels that can be assembled on site and act as formwork for the in situ casting of the concrete core. As well, they exhibit superior behavior characteristics, particularly with respect to dynamic response and impact resistance.

The nuclear power industry was a driving force in the design, development and use of SC wall systems. Research activity in this area was extensive in the late 1980s and early to mid 1990s. As the construction of new nuclear power plants abated worldwide at the turn of the century, research interest declined. However, a resurgence in the design and construction of nuclear plants has resulted in renewed interest in SC wall systems. Use of SC walls has also expanded to other applications such as concrete gravity

based offshore structures and blast and impact resistance protective structures.

For the modeling of SC wall elements, two general approaches are available. For the analyses of simple structures, effective analytical models have been developed based primarily on strut and tie methods and internal truss conceptualizations. For the analyses of more complex structures, finite element analysis (FEA) procedures have been applied.

With finite element analyses, the common approach is to use powerful general purpose software packages and apply them in a micro-modeling of the wall details. That is, the finite element meshes are typically so finely detailed as to model individual anchor studs and tie-bars as well as the concrete and steel continuums in a full three-dimensional representation. Interface elements are also typically used to capture the effects of contact/bond stresses and interfacial slip. However, this approach has met with only limited success for two reasons. First, the micro-modeling approach is complex, time consuming and expensive both in the preparation of the models and in the computational demand; large structural systems represent a significant challenge. Secondly, the commercial software typically available for these purposes has shown difficulty in accurately capturing the response of concrete, particularly in brittle shear-critical situations.

Thus, a need exists for improved finite element analyses of steel concrete composite elements. The smeared modeling approach, as has been developed by several researchers for the simulation of RC structures, has the potential for simplifying the modeling process and decreasing the computational demand. Moreover, the incorporation of models more sensitive to the complex nuances in concrete

\* Corresponding author. Tel.: +1 416 978 5910; fax: +1 416 978 6813.  
E-mail address: [fjv@civ.utoronto.ca](mailto:fjv@civ.utoronto.ca) (F.J. Vecchio).

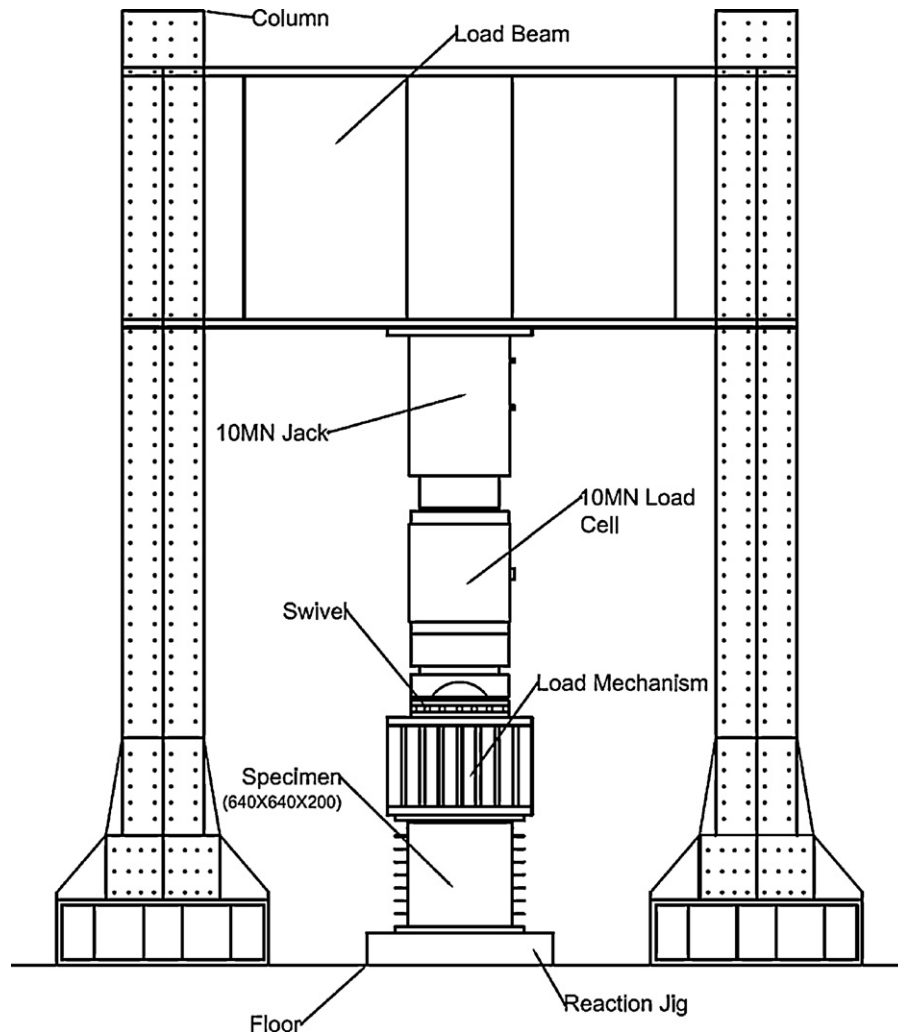


Fig. 1. Set-up used by Usami et al. (1995) to test SC panels in compression.

constitutive behavior hold the potential for improved accuracy in the calculation of SC element response.

The Modified Compression Field Theory (MCFT) (Vecchio and Collins, 1986) was developed as a simple behavioral model for cracked reinforced concrete planar elements. It utilizes a smeared rotating crack concept, incorporating specially developed constitutive models for cracked reinforced concrete based on data obtained from a comprehensive series of panel element tests. The MCFT has demonstrated good accuracy in simulating structural response in most situations (Vecchio et al., 1996), particularly for difficult cases where the structures are shear-critical. It has subsequently been implemented in various finite element analysis algorithms and in several design codes (e.g., CSA A23.3 (CSA, 2004), the U.S. Highway Bridge Design Code, and the European Model Design Code (CEB FIP, 1990)).

The Disturbed Stress Field Model (DSFM) (Vecchio, 2000) was subsequently developed as a refinement of the MCFT, allowing for various complexities in behavior not considered by the MCFT. It is also better suited to finite element implementation.

In this study, the DSFM is adapted to the analysis of SC elements. The adapted model is then implemented into a 2D nonlinear finite element analysis algorithm. Verification studies are undertaken to investigate the accuracy of the analysis approach, examining its ability to model the behavior of simple and complex SC test specimens reported in the literature. Conclusions and recommendations are drawn accordingly.

## 2. Previous research on SC elements

Usami et al. (1995) examined the compression response of SC elements with particular attention paid to the buckling characteristics of the faceplates. Four panels were tested under cyclic uniaxial compression of progressively increasing magnitude using the test set up depicted in Fig. 1. The prime variable in the test program was the ratio of the anchor stud spacing ( $b$ ) to the plate thickness ( $t_s$ ), ranging from 20 to 50. Test observations of plate buckling were compared against predictions obtained from the classical Euler buckling equation. It was found that for elements where the Euler buckling stress was less than  $0.6f_y$ ,  $f_y$  being the yield stress of the steel, the Euler expression gave reasonably accurate results. For cases where the buckling stress was greater than  $0.6f_y$ , the Euler expression overestimated the buckling stresses. For the case of  $b/t_s = 20$ , the calculated buckling stress was approximately equal to the plate yield stress.

Ozaki et al. (2004) described experimental investigations performed on 16 SC panels subjected to shear. The panels were tested using a specially devised test rig in which load was applied at anchor points along each edge of the panel (see Fig. 2), attempting to simulate a condition of uniform edge stresses. Test parameters included specimen type, type of loading, and material properties. For all specimens, the ratio of the stud spacing to plate thickness,  $b/t_s$ , was 30. Test results showed that, as one might expect, the element strength and stiffness increased with faceplate thickness. As

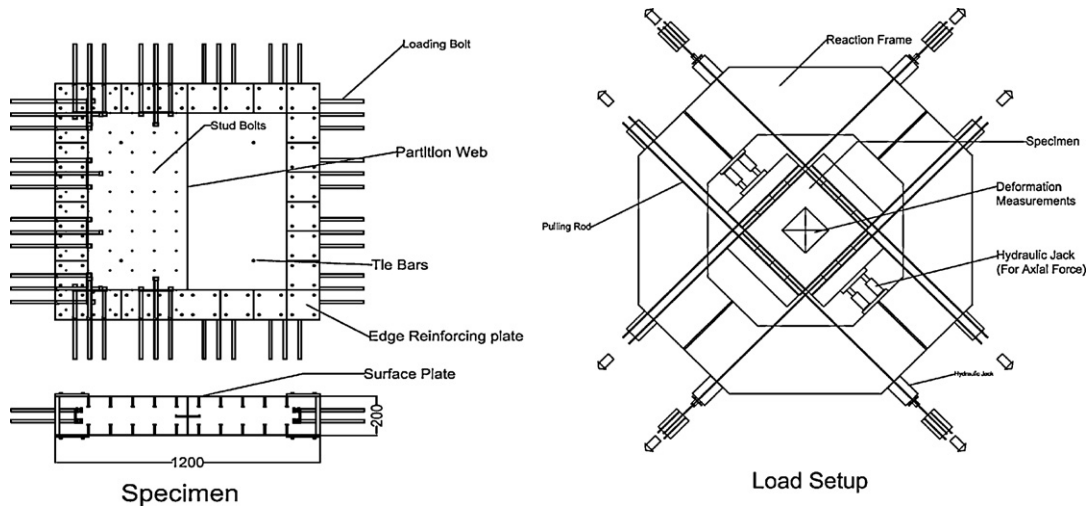


Fig. 2. Specimen configuration and loading apparatus for Ozaki et al. (2004) SC shear panels.

well, applied axial compression improved the shear response of the elements. Plate buckling was not observed to occur, and thus had no influence on the behavior. Ozaki et al. (2004) developed analytical formulae, utilizing effective moduli for concrete pre- and post-cracking stiffness and steel plate pre- and post-yield stiffness, combined with a post-cracking equivalent truss model, to describe the nominal response of the panels. These formulations built on earlier models developed by Ozaki et al. (2001).

Takeda et al. (1995) also performed studies on seven SC panels subjected to pure shear, utilizing the same specimen configuration and test apparatus as subsequently used by Ozaki et al. (2004). This test series focused on panels with web partitions (i.e., diaphragms) in which the partitions contained no stud anchors. Number of partitions, stud configuration, and thickness of the faceplates were the main variables. The typical failure mode of these panels involved cracking of the concrete, followed by pre-yield buckling of the steel faceplates in the compression direction, and concluded with yielding of the faceplates in the tension direction and crushing of the concrete in compression. A simple quadra-linear response model was developed, also based on effective material moduli and an ‘equivalent truss’ analogy. While somewhat conservative, the model gave reasonably accurate calculations of the cracking and ultimate stress capacities.

Sasaki et al. (1995) tested flanged shear wall specimens under in-plane lateral loading conditions. A total of seven specimens were tested, varying in height and web thickness. The flanged shear wall specimens were constructed integral with top and base blocks (see Fig. 3). A regime of reversed cyclic lateral displacement was applied

to the top block. As well, one specimen had co-acting axial load, and another varied in the nature of the stud anchor pattern used. The specimens exhibited a marginally ductile response governed by yielding and then buckling of the web faceplates and compression shear failure of the web concrete. Story drifts of about 2.5% to 4.0% were attained. The authors concluded that the specimens exhibited superior performance compared to equivalent RC walls.

Suzuki et al. (1995) developed an analytical strut and tie model (STM) based on a lower bound limit analysis, to model the behavior of the Sasaki shear walls. The proposed formulation combined a truss model similar to that of Ozaki et al. (2004) with an ‘arch mechanism’ model accounting for the contribution of the flanges. Good agreement with experimental results was reported.

Rectangular cross section shear wall specimens were tested by Takeuchi et al. (1995). Their test set-up used a swivel loading apparatus to induce shear loading while simultaneously applying an axial compression. The web panels of the test specimens were 600 mm high by 640 mm wide, 200 mm thick, and with 3.2 mm thick faceplates. The  $b/t_s$  ratio (stud spacing to plate thickness ratio) for the faceplates was a primary variable; plates with  $b/t_s$  values of 20, 30, 40 and 50 were utilized. In these tests, plate buckling was found to occur in some specimens, highlighting the importance of using adequate stud details to improve the performance of the elements. This test program concluded with the testing of a flanged shear wall specimen. While the specimen exhibited good ductility, it was able to achieve only 70–80% of the anticipated load capacity with a localized failure in the compression toe of the wall. A basic composite stiffness formulation, somewhat similar to that devel-

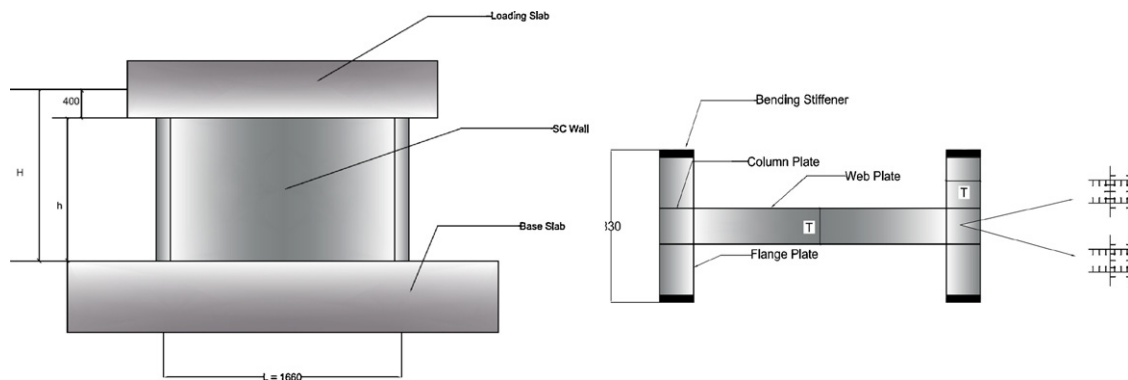


Fig. 3. Flanged shear wall specimens tested by Sasaki et al. (1995).

oped by Ozaki et al. (2004), was used to calculate the theoretical response.

Eom et al. (2009) tested five large scale slender double skin composite walls with tie-bars, including both single walls and coupled walls, to investigate seismic behavior under reversed cyclic lateral load conditions. The authors concluded from the test results that such walls have excellent load carrying capacity. However they also found that, in order to ensure a ductile behavior and prevent early fracture of the welded connections at the base of the wall or at the interfaces of the coupling beams, special attention to the connection details was required. The use of a strengthening plate at the connections was recommended. When early tensile fracture in the welded connections was averted, the walls failed primarily from local buckling of the steel plates because of the plastic residual strains developed in the steel plates under cyclic loading. In walls with a tie-bar to plate thickness ratio of 30, local buckling of the steel plates was initiated at strains of about  $25 \times 10^3$ .

Significant experimental studies also have been reported by Wright et al. (1991), Driver et al. (1998), Hajjar (2002), Liang et al. (2004) and others.

Zhou et al. (2010) described the application of finite element procedures to assessing the seismic performance of a composite steel-concrete wall previously tested, one of the few such studies available in the literature. Their approach was to apply a grid of steel plate elements overtop a grid of plane stress elements representing the concrete core. The steel plate elements were tied to the concrete elements only at the locations of shear studs at which points perfect bond was enforced. The stiffened top and side edge portions of the wall were represented using beam/column elements. The material modeling of the concrete core was done according to the Cyclic Softened Membrane Model (CSMM). The authors reported good agreement for the pre-cracking stiffness, post-cracking stiffness, ultimate strength, residual displacement, and energy dissipation of the wall.

The formulation presented herein differs from that employed by Zhou et al. (2010) in that the concrete and steel components are considered integrally in the development of the element constitutive response. Not only does this result in easier modeling of SC structures, it allows for better consideration of interaction effects between the two components (such as tension stiffening effects and concrete crack spacing and widths).

### 3. Formulation of analysis model

To facilitate the analysis of steel-concrete (SC) composite sandwich panels, the Disturbed Stress Field Model (DSFM) (Vecchio, 2000) will be used as the theoretical basis and modified accordingly. The DSFM is an extension of the Modified Compression Field Theory (MCFT) (Vecchio and Collins, 1986), developed to describe the behavior of cracked reinforced concrete elements subjected to in-plane forces.

The MCFT is essentially a fully rotating smeared crack model that represents concrete as an orthotropic material. Equilibrium, compatibility, and stress-strain relationships are formulated in terms of average stresses and average strains. However, also central to the theory is the examination of local stress conditions at crack locations. In the MCFT formulation, cracked reinforced concrete is treated as distinctly different from plain concrete, with constitutive relations and failure criteria derived from comprehensive series of panel element tests. An essential aspect of the MCFT is its consideration of concrete compression softening and concrete tension stiffening effects. The concrete compression softening relationships developed and integrated into the model reflect the observation that cracked concrete, when simultaneously subjected to high tensile strains in the direction normal to the compression,

exhibits significantly reduced strength and stiffness relative to uncracked uniaxially compressed concrete. Compression softening has a significant influence on the computed strength of shear-critical elements. The tension stiffening formulations implemented represent the influence of post-cracking average tensile stresses in the concrete between cracks. Tension stiffening significantly influences the calculated deflection response of concrete elements.

The DSFM was developed as a refinement of the MCFT for implementation in nonlinear finite element algorithms. Unlike the MCFT, it explicitly considers slip mechanisms on crack surfaces and their contribution to element deformation, and deviations between principal stress and principal strain directions within the concrete. Further, it allows for the consideration of post-cracking Poisson's effects, elastic strain offsets due to such actions as thermal expansion or concrete drying shrinkage, and plastic strain offsets due to loading history or yielding or damage of the materials. As well, some refinements are made to the constitutive relations for compression softening and tension stiffening. Herein, the DSFM is expanded to include the modeling of SC elements.

Consider a double-skinned SC element composed of a concrete core of thickness  $t_c$  and two steel faceplates each of thickness  $t_s$ . For the sake of generality, although it is seldom the case, assume that the SC element contains conventional in-plane reinforcement (i.e., rebar) as well. The element is subjected to the in-plane stress condition  $[\sigma] = \{\sigma_x, \sigma_y, \tau_{xy}\}$  as shown in Fig. 4. Accordingly, the element experiences a total average strain condition represented by  $[\varepsilon] = \{\varepsilon_x, \varepsilon_y, \varepsilon_{xy}\}$ . The average inclination of the principal strains in the element is given by:

$$\theta_\varepsilon = \frac{1}{2} \tan^{-1} \left[ \frac{\gamma_{xy}}{\varepsilon_x - \varepsilon_y} \right] \quad (1)$$

The deformation of the concrete component of the element can be considered to be the sum of a continuum strain and local rigid body slip along crack surfaces. The total average strains in the concrete can thus be defined according to the following relation:

$$[\varepsilon] = [\varepsilon_c] + [\varepsilon_c^e] + [\varepsilon_c^p] + [\varepsilon_c^s] \quad (2)$$

where  $[\varepsilon_c]$  are net strains in the concrete,  $[\varepsilon_c^e]$  are elastic offset strains in the concrete (accounting for such actions as thermal expansion, drying shrinkage, and pre- and post-cracking Poisson's effects),  $[\varepsilon_c^p]$  are plastic offset strains (accounting for non-recoverable strains to loading/unloading and damage), and  $[\varepsilon_c^s]$  are the strains associated with slip on the cracks (i.e., rigid body slip).

Assume that the element contains any number ( $i = 1, \dots, n$ ) of in-plane reinforcing bar components, provided at an inclination of  $\alpha_i$  and having a reinforcement ratio, relative to the concrete core, of  $\rho_i$ . It is assumed that the reinforcement is perfectly bonded to the concrete. Thus, the strain condition of the reinforcement can be described as:

$$[\varepsilon] = [\varepsilon_r]_i + [\varepsilon_r^e]_i + [\varepsilon_r^p]_i \quad (3)$$

where  $[\varepsilon_r]_i$  are net strains in the reinforcement component,  $[\varepsilon_r^e]_i$  are elastic offset strains in the reinforcement (accounting for such actions as thermal expansion or prestressing), and  $[\varepsilon_r^p]_i$  are plastic offset strains in the reinforcement (accounting for plastic yield strains and Bauschinger effects).

Similarly, for the steel faceplate component of the element, the total strain condition can be defined as:

$$[\varepsilon] = [\varepsilon_s] + [\varepsilon_s^e] + [\varepsilon_s^p] \quad (4)$$

where  $[\varepsilon_s]$  are net strains in the steel component,  $[\varepsilon_s^e]$  are elastic offset strains in the reinforcement (accounting for such actions as thermal expansion and Poisson's effects), and  $[\varepsilon_s^p]$  are plastic offset strains in the steel (accounting for plastic yield strains and Bauschinger effects).

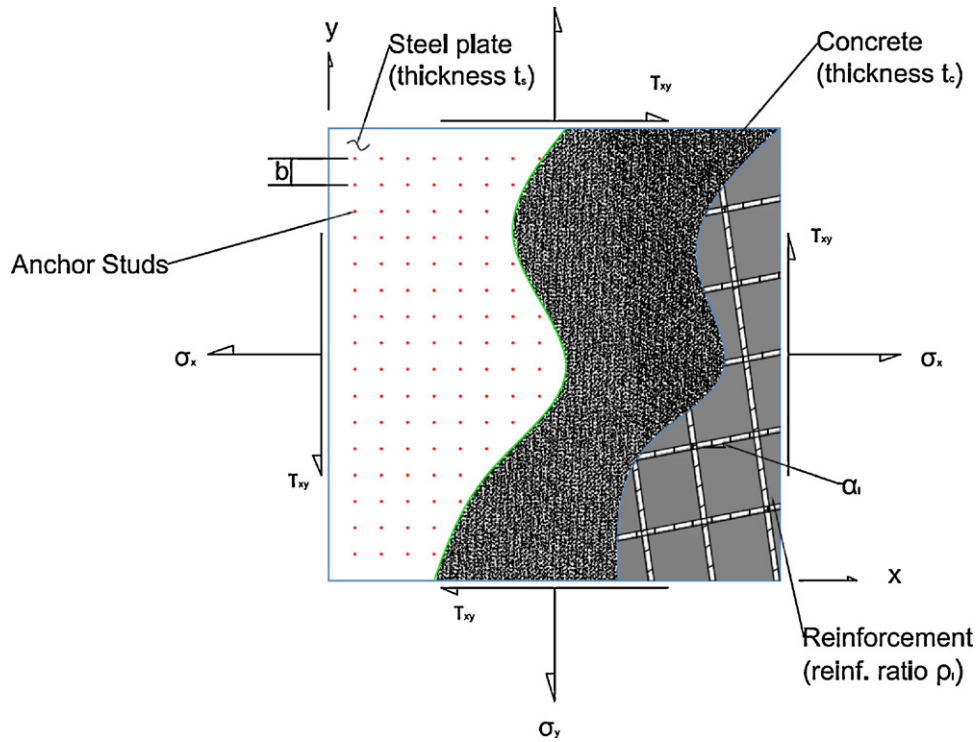


Fig. 4. SC panel element subjected to in-plane stresses.

Thus, the constitutive response of the element can be defined by

$$[\sigma] = [D][\varepsilon] - [\sigma^0] \quad (5)$$

where  $[D]$  is the composite material stiffness matrix and  $[\sigma^0]$  is a 'prestress' vector. The composite material stiffness matrix is the summation of the component stiffness matrices for the concrete, reinforcement, and steel, as follows:

$$[D] = \frac{t_c}{(t_c + 2t_s)} [D_c] + \sum_{i=1}^n \frac{t_c}{(t_c + 2t_s)} [D_r]_i + \frac{2t_s}{(t_c + 2t_s)} [D_s] \quad (6)$$

The prestress vector  $[\sigma^0]$  is defined as

$$[\sigma^0] = [D_c]([\varepsilon_c^e] + [\varepsilon_c^p] + [\varepsilon_c^s]) + \sum_{i=1}^n [D_r]_i([\varepsilon_r^e]_i + [\varepsilon_r^p]_i) + [D_s]([\varepsilon_s^e] + [\varepsilon_s^p]) \quad (7)$$

The concrete component material stiffness matrix,  $[D_c]$ , is evaluated with respect to the principal stress directions of the concrete, which may differ from the principal strain directions, and transformed back to the reference  $x, y$  axes system. A secant stiffness approach is taken in defining the effective moduli in the principal directions, using appropriate constitutive relations for concrete. The complete formulation of  $[D_c]$  is described by Vecchio (2000, 2001). It should be noted that the DSFT formulation includes models accounting for concrete compression softening effects, concrete tension stiffening effects, pre- and post-cracking Poisson's effects, and confinement effects.

Similarly, a component material stiffness matrix  $[D_r]_i$  is defined for each reinforcement component according to appropriate constitutive relations and using a secant stiffness approach. The formulation allows for the consideration of yielding, Bauschinger effects, and dowel action. Again, a complete description of the formulation is given by Vecchio (2000, 2001).

To be consistent with the DSFM approach, the material stiffness matrix for the steel faceplates must be defined as a diagonal matrix with respect to the principal stress directions which are assumed to coincide with the principal strain directions of the element, defined by  $\theta_\varepsilon$ . Thus, with respect to the principal directions,

$$[D_s]' = \begin{bmatrix} \bar{E}_{s1} & 0 & 0 \\ 0 & \bar{E}_{s2} & 0 \\ 0 & 0 & \bar{G}_s \end{bmatrix} \quad (8)$$

where  $\bar{E}_{s1}$ ,  $\bar{E}_{s2}$ , and  $\bar{G}_s$  are secant moduli. For a particular stress-strain state, the secant moduli are evaluated as follows:

$$\bar{E}_{s1} = \frac{f_{s1}}{\varepsilon_{s1}}, \quad \bar{E}_{s2} = \frac{f_{s2}}{\varepsilon_{s2}}, \quad \bar{G}_s = \frac{\bar{E}_{s1} \cdot \bar{E}_{s2}}{\bar{E}_{s1} + \bar{E}_{s2}} \quad (9)$$

the strains  $\varepsilon_{s1}$  and  $\varepsilon_{s2}$  are net principal strains in the steel plate determined from the steel net strain vector  $[\varepsilon_s]$  using standard transformations. The stresses  $f_{s1}$  and  $f_{s2}$  are determined from the respective strains using appropriate uniaxial stress-strain relationships for steel allowing for yielding, strain hardening and, in the case of reversed cyclic loading, Bauschinger's effect. For the backbone monotonic response, a tri-linear elastic-plastic strain hardening response is assumed.

The steel material stiffness matrix  $[D_s]'$  is transformed back to the reference  $x, y$  reference system to obtain  $[D_s]$ :

$$[D_s] = [T_s]^T [D_s]' [T_s] \quad (10)$$

where the transformation matrix  $[T_s]$  is given by

$$[T] = \begin{bmatrix} \cos^2 \theta_\varepsilon & \sin^2 \theta_\varepsilon & \cos \theta_\varepsilon \sin \theta_\varepsilon \\ \sin^2 \theta_\varepsilon & \cos^2 \theta_\varepsilon & -\cos \theta_\varepsilon \sin \theta_\varepsilon \\ -2 \cos \theta_\varepsilon \sin \theta_\varepsilon & 2 \cos \theta_\varepsilon \sin \theta_\varepsilon & (\cos^2 \theta_\varepsilon - \sin^2 \theta_\varepsilon) \end{bmatrix} \quad (11)$$

In this formulation, Poisson's effects for steel are incorporated as elastic offsets, handled in the same manner as described by Vecchio (1992) for concrete pre- and post-cracking expansion effects. Thus,

with respect to the principal stress/strain direction ( $\theta_\varepsilon$ ), the elastic offset strains  $\varepsilon_{s1}^e$  and  $\varepsilon_{s2}^e$  are defined as:

$$\varepsilon_{s1}^e = -\nu \cdot \varepsilon_{s2}, \quad \varepsilon_{s2}^e = -\nu \cdot \varepsilon_{s1} \quad (12)$$

where  $\nu$  is Poisson's ratio (assumed to be constant at 0.30 both before and after yield), and  $\varepsilon_{s1}$  and  $\varepsilon_{s2}$  are the net principal strains. The elastic offset strains are then transformed back to the reference ( $x, y$ ) axis system and added to the elastic offset vector [ $\varepsilon_\varepsilon^e$ ].

To consider yielding of the steel plates under general biaxial stress conditions, the von Mises criterion is used. Thus, for steel with a uniaxial yield strength  $f_y$ , the yield criterion is given by:

$$(f_{s1} - f_{s2})^2 + (f_{s2} - f_{s3})^2 + (f_{s3} - f_{s1})^2 = 2(f_y)^2 \quad (13)$$

where  $f_{s1}$ ,  $f_{s2}$ , and  $f_{s3}$  are principal stresses in the plate. Being a surface plate with predominantly in-plane stresses acting, one of the principal stresses will be zero.

There are a number of interaction effects between the concrete and the steel plates that should be considered, including: influence of the steel plates on average crack spacing in the concrete, influence of the steel plates on concrete tension stiffening effects, interfacial slip between the plates and the concrete due to deformation of the anchor studs, buckling of the steel faceplates at advanced stages of compression, and out-of-plane confinement of the concrete in the case of tied faceplates.

No experimental data is available in regards to the contribution that steel plates in SC elements provide towards concrete tension stiffening effects. The general rule of thumb with conventional rebar, however, is that the influence extends to a zone of about 7.5 bar diameters from the rebar. With the relatively thin plates used in SC elements, this zone typically represents a small portion of the overall concrete core thickness. Moreover, the bond characteristics of the plates will be less favorable than that of fully embedded deformed rebar. Thus, in the absence of more definitive data, it will be assumed that the steel faceplates make no contribution to concrete tension stiffening effects.

Various crack spacing formulations are available for reinforced concrete; the formulation used in the DSFM is based on the model presented in the *fib* Model Code (CEB FIP, 1990). However, that formulation depends heavily on rebar characteristics such as diameter and cover and is not easily adaptable to the consideration of steel surface plates. In the Canadian Design Code A23.3 (CSA, 2004), the maximum crack spacing is limited to the distance between layers of crack control reinforcement. Where none is provided other than the main flexural reinforcement, the maximum crack spacing is set as the effective depth of the member. Thus, it will be assumed that, for SC elements containing no in-plane reinforcement, the maximum crack spacing is approximately equal to the thickness of the element.

For steel faceplates with a stud spacing to plate thickness ratio of  $b/t_s$ , Usami et al. (1995) reported that the critical buckling stress in compression ( $\sigma_{cr}$ ) can be approximated by the following modified Euler expression:

$$\sigma_{cr} = \frac{\pi^2 E_s}{12n^2(b/t_s)^2} \quad (14)$$

where  $n = 0.7$  and  $E_s$  is the modulus of elasticity of the steel. This formulation is thus implemented in the computational model. When the stress in the principal compression direction exceeds the critical stress, the plate is assumed to have buckled and the stress carried in compression thereafter is assumed to be zero.

The hysteretic behavior of concrete under reversed cyclic loading, for the analyses reported herein, is modeled according to the basic nonlinear formulation described by Vecchio (1999). For a more comprehensive treatment, better capturing the effects of cyclic damage, the model proposed by Palermo and Vecchio (2003)

is available. The hysteretic response of the rebar steel and plate steel, including the Bauschinger effect, is represented by the formulation proposed by Seckin and modified by Vecchio (1999). With respect to the response of plate steel after compression buckling, it is assumed that the steel can re-enter the tension regime normally but can no longer sustain stresses in compression during load reversals. Note too that the compression buckling stress is likely influenced by reversed cyclic loading, particularly if plastic offset strains develop during a preceding tension excursion; however, this influence is currently not taken into account in the use of Eq. (14). A more rigorous buckling formulation can be patterned after the model of Dhakal and Maekawa (2002).

Finally, for this preliminary formulation, it will also be assumed that the anchor studs provided are sufficient to limit the amount of interfacial slip between the concrete and the plates to negligible levels.

The SC element formulation described above was implemented into program VecTor2, a nonlinear finite element program originally developed for the analysis of two-dimensional planar reinforced concrete structures (Vecchio, 1989, 1990). VecTor2 fully incorporates the smeared rotating crack approach and constitutive modeling described by the MCFT and DSFM. The program's solution algorithm is based on a secant stiffness formulation using a total load iterative procedure, giving it numerically robust and stable performance with good convergence characteristics. The DSFM based formulation for SC elements was implemented using the same algorithm as described by Vecchio (2001) for RC elements.

#### 4. Verification studies

The adequacy of the SC analysis model developed, and its implementation into a nonlinear finite element analysis algorithm, will be tested by modeling the response of specimens from three series of tests. The test specimens cover a diverse range of structural geometries, loading conditions and governing behavior mechanisms, from simple to complex, and thus represent a stringent test of the accuracy of the formulations.

It should be noted that in all the analyses that follow, all analysis parameters and material modeling options were set to the default values of the analysis program VecTor2. No fine tuning of the analysis parameters, material modeling or structural modeling was undertaken. All results presented here are essentially 'first run' results.

##### 4.1. Uniaxial compression panels

Usami et al. (1995) tested four SC panels under uniaxial compression, with the primary intent of studying the effects of plate buckling, using the test set up shown in Fig. 1. The test panels were 640 mm × 640 mm × 200 mm in size with 3.24 mm thick faceplates and 5.95 mm thick side plates. Specimens NS20, NS30, NS40 and NS50 varied in the ratio of anchor stud spacing to plate thickness ( $b/t_s$ ), with values of 20, 30, 40 and 50, respectively. The concrete had a compressive strength of 31.2 MPa, a modulus of elasticity of 22,800 MPa, and a maximum aggregate size of 10 mm. The faceplate steel was characterized by a yield strength of 287 MPa, an ultimate strength of 427 MPa, and a modulus of elasticity of 196,000 MPa. The side plate steel had a yield strength of 366 MPa, an ultimate strength of 465 MPa, and a modulus of elasticity of 208,000 MPa. The Poisson's Ratio for the concrete was measured as 0.18, and for the faceplate and side plate steels as 0.28.

According to the Euler expression for plate buckling suggested by Usami et al. (1995), the buckling stresses for the panel faceplates were 822 MPa, 366 MPa, 206 MPa, 132 MPa for Panels NS20, NS30, NS40, and NS50, respectively. Given that the faceplate steel yield

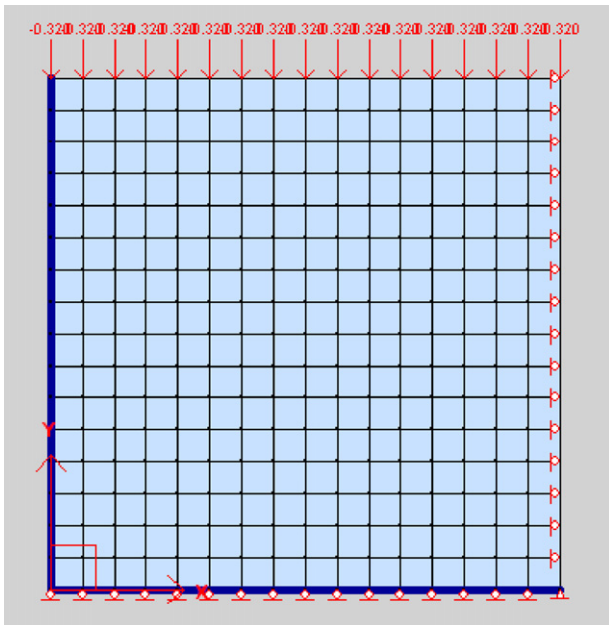


Fig. 5. Finite element model for Usami et al. (1995) compression panels.

stress was 287 MPa, one would expect only the latter two panels to exhibit plate buckling prior to yielding in compression. From test observations, Usami et al. reported plate yielding for NS20, and plate buckling for NS30, NS40, and NS50. In all cases, the final failure mode involved a moderately brittle compression crushing of the concrete.

For finite element analysis of the test panels, taking advantage of double symmetry, one quarter of each panel was modeled using the mesh shown in Fig. 5. The SC panel was modeled using 8 dof rectangular elements (using the SC formulation described above) and the side plates were represented with 4 dof truss bar elements. The modeling assumed a frictionless support condition at the loading platens; thus roller supports were provided along the bottom edge. Loads were applied as monotonically increasing nodal displacements along the top edge. The material properties were set to those provided by Usami et al.

Since the Euler expression was incorporated into the modeling, the FE analysis results obtained were consistent with that formulation; that is, plate yielding was predicted for Panels NS20 and NS30, and plate buckling was calculated for Panels NS40 and NS50. In the case of Panel NS40, plate buckling was calculated to occur at a load of 3372 kN, reasonably consistent with the first observed buckling in the experiment at a load of 3560 kN. For Panel NS50, the predicted plate buckling occurred at 2264 kN, versus the 2160 kN load at which first buckling was observed in the test. In the analyses, all panels sustained a brittle compression failure of the concrete, consistent with the test observations. Although the final failure exhibited localization, all elements achieved peak and post-peak response.

The calculated load capacities of the panels compare well with those measured, as evident in Table 1. For the four panels, the ratio of the predicted to measured load capacity had a mean of 1.04 and

Table 1  
Load capacities of compression panels.

Specimen	$P_{u-Test}$ [kN]	$P_{u-calc}$ [kN]	$P_{u-calc}/P_{u-Test}$
NS20	5730	5888	1.027
NS30	5470	5888	1.076
NS40	5000	5169	1.034
NS50	5050	5153	1.020

Table 2  
Shear panel specimen parameters.

Specimen	$t_s$ [mm]	$\sigma_n$ [MPa]	$f'_c$ [MPa]	$E_c$ [MPa]	$f_y$ [MPa]	$E_s$ [MPa]
S200NN	2.30	0.00	42.2	27,200	340	197,000
S215NN	2.30	1.47	41.6	27,700	340	197,000
S230NN	2.30	2.94	42.0	27,900	340	197,000
S300NN	3.20	0.00	41.9	27,600	351	199,000
S315NN	3.20	1.47	41.6	26,700	351	199,000
S330NN	3.20	2.94	40.1	27,000	351	199,000
S300PS	3.20	0.00	41.9	27,100	351	199,000
S300PN	3.20	0.00	39.9	27,200	351	199,000
S400NN	4.50	0.00	42.8	27,600	346	207,000

a coefficient of variation of 2.4%. Note that while a cyclic loading regime was used at the early and intermediate stages of loading in the test panels, the analyses were done with monotonically increasing displacement. The cycling may have induced some hysteretic damage to the concrete, possibly reducing the load capacities and thus accounting for some of the discrepancy. By comparison, using their analytical model based on an effective stiffness formulation, Usami et al. (1995) obtained a mean of 0.92 and a coefficient of variation of 4.1% for the strengths of these panels. The panels' nominal capacity, based on cross sectional areas and material strengths, was 5850 kN.

The computed load-deflection responses for the panels are compared to the experimentally measured responses in Fig. 6. Generally, the pre-peak responses correlate reasonably well, with the deflection at peak load better simulated than that obtained from the analytical model of Usami et al. (1995). The calculated post-peak response is somewhat more brittle than observed, owing to the fact that the parabolic stress–strain base curve used as the default for concrete in compression underestimates post-peak ductility of both confined and unconfined concrete. It is also interesting to note that for Panels NS40 and NS50, the momentary slight drop in load partway up the ascending portion of the calculated response corresponds to the occurrence of plate buckling. Usami indicated that, during the tests, there was no major drop in load at the instance of plate buckling.

#### 4.2. Shear panels

Ozaki et al. (2001, 2004) performed shear tests on a number of SC panels, all 1200 mm × 1200 mm × 200 mm in dimension. The panels were loaded using a specially devised test rig in which tangential forces were applied at several discrete anchor points along each edge of the panel (see Fig. 2), simulating a condition of uniform edge stress. Test parameters included specimen type (i.e., solid panels, panels with perforations, and panels with partition plates), type of loading (i.e., pure shear, and shear combined with axial load), and material properties (i.e., faceplate thickness, and material strengths). For all specimens, the ratio of the stud spacing to plate thickness,  $b/t_s$ , was 30. Around the perimeter, thickened steel plates and reinforcement anchors were used to help transfer force from the loading actuators and test rig to the panel without inducing edge failures.

Here, the nine solid panels without perforations will be examined. Panel details and material strengths are given in Table 2. The NN series panels contained no partition (diaphragm) plates. Panel S400PS had a center partition plate with anchor studs. Panel S400PN had a similar partition plate but with no anchor studs. The compressive strengths ( $f'_c$ ) and moduli of elasticity ( $E_c$ ) of the concrete in the panels were reported as shown in Table 2. The maximum aggregate size was 10 mm. The yield strengths ( $f_y$ ) and moduli of elasticity ( $E_s$ ) of the faceplate steel are also given in Table 2; the plate thicknesses are shown as  $t_s$ . The panels were subjected to reversed cyclic shear. Some panels were subjected to constant co-acting uniaxial compressive stress ( $\sigma_n$ ); see Table 2.

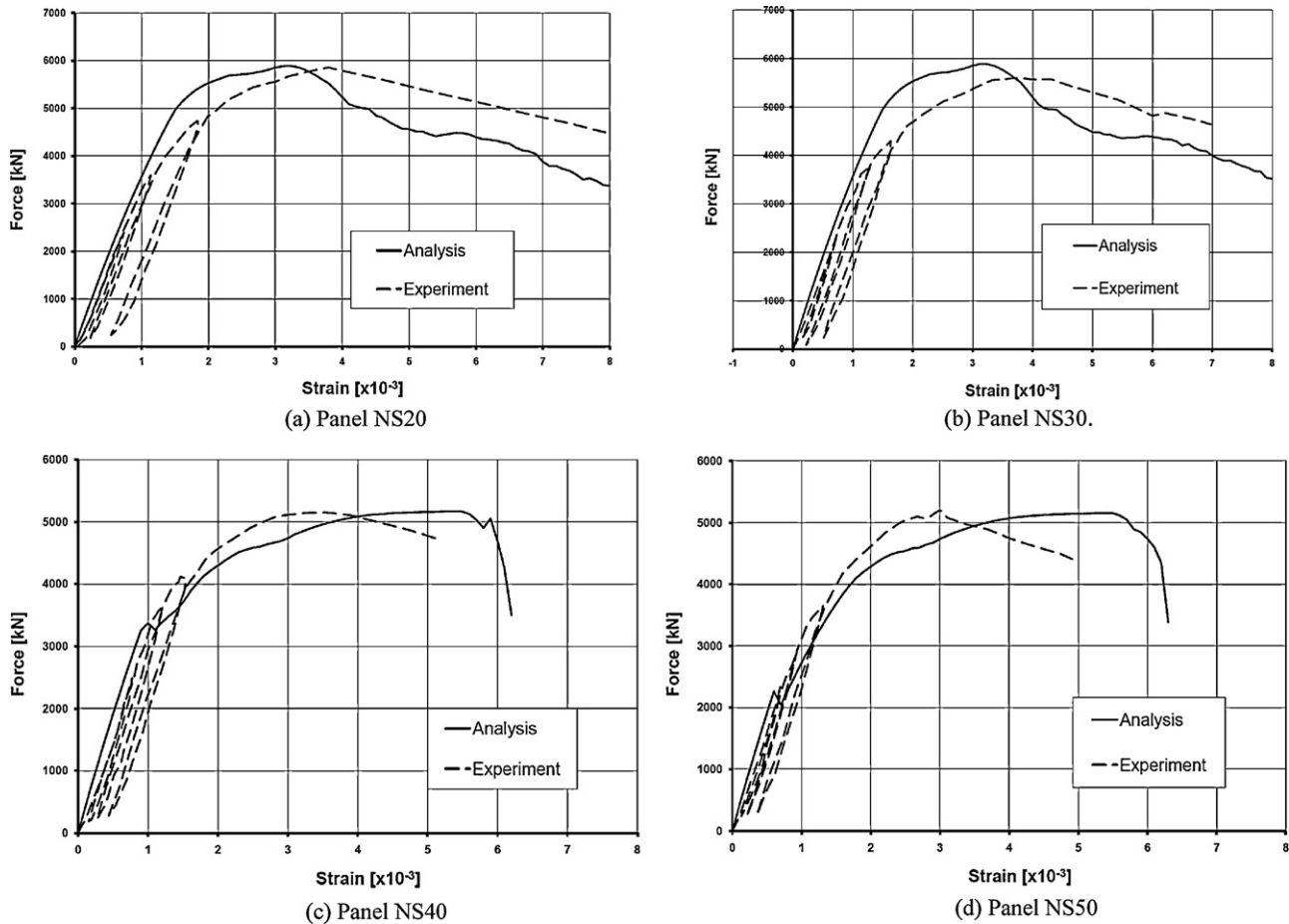


Fig. 6. Load-deflection responses for Usami et al. (1995) compression panels.

From the experiments, it was observed that these test panels exhibited a generally ductile response, governed by yielding of the faceplate in tension and then crushing of the concrete in the principal compression direction. As the faceplate thickness amongst the specimens increased, the core concrete was subjected to higher levels of compression and thus ductility was reduced. Co-acting axial compression was found to increase the cracking load, but to have only a minor effect on the yield and ultimate loads. The partition walls were also found to have little influence on the yield and ultimate capacities. Buckling of the faceplates before yielding was not observed.

The element mesh used to model the typical panel is shown in Fig. 7; note that an attempt was made to model the thickened plates and the in-plane and out-of-plane reinforcement used at the loading points. One corner pin support (bottom left) and one corner roller support (bottom right) were used to render the model statically determinate. Shear loads were applied as uniform tangential nodal forces along the edges of the panel. For panels with co-acting axial compression, horizontal nodal forces were applied on the vertical faces, creating the axial compression in the  $x$ -direction.

The center partition plate in Panel S300PS was modeled using truss bar elements. Since this plate had anchor studs on both sides along its length, the truss elements were modeled assuming perfect bond to the concrete. In Panel S300PN, the partition plate had no anchor studs. Thus, it was modeled as unbonded reinforcement, using truss bar elements and link elements where the bond stress slip relationship for the link elements was set to zero.

The strengths and moduli of elasticity of the concrete and steel used in modeling the panels were as given by Ozaki et al. (2004).

Poisson's ratios of 0.15 and 0.30 were assumed for the concrete and faceplate steel, respectively. All faceplate steel was assumed to have an ultimate strength ( $f_u$ ) of 480 MPa and a rupture strain ( $\epsilon_u$ ) of  $40 \times 10^3$ .

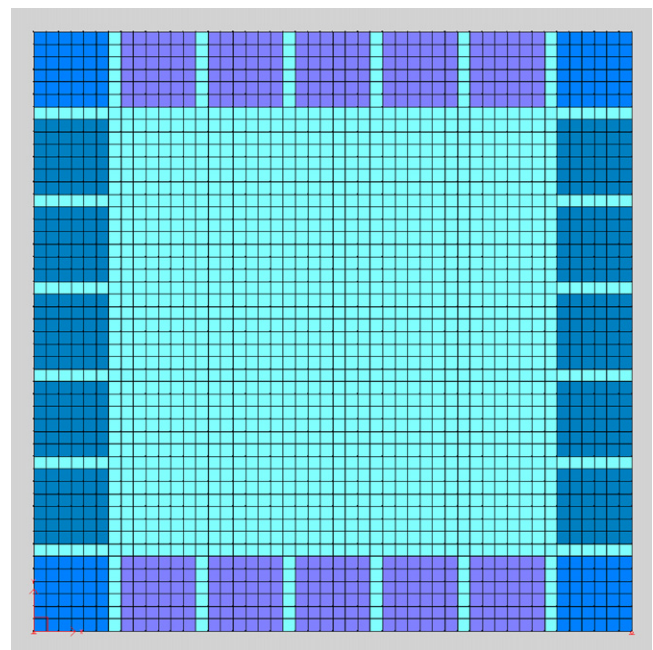


Fig. 7. Typical finite element mesh used for Ozaki et al. (2004) shear panels.

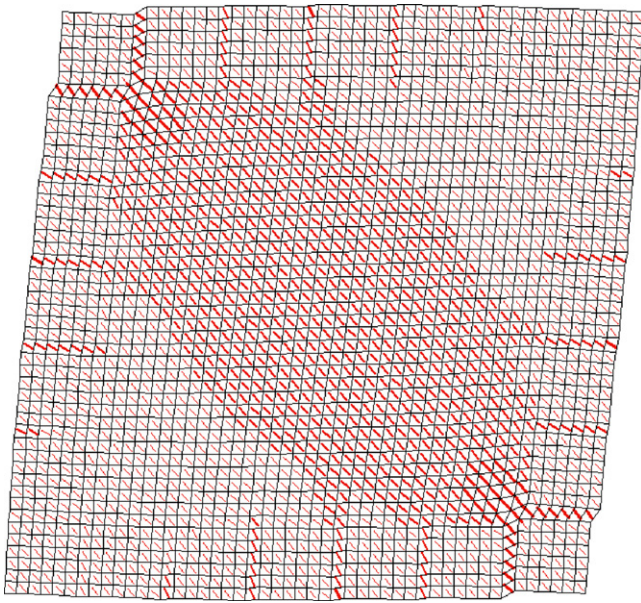


Fig. 8. Crack pattern and deflected shape [20 $\times$ ] of Panel S300NN at ultimate load.

The analyses were conducted with the total applied shear force per side,  $Q$ , increased monotonically until failure. A load step size of  $\Delta Q = 24$  kN (equivalent to a nominal shear stress of 0.10 MPa) was used. Note that the loading was performed in a force-controlled mode; a displacement-controlled loading procedure was not possible for this test arrangement. Thus, when the calculated load capacities of the specimens were exhausted, the specimens failed abruptly; no post-peak load deflection responses could be calculated for these specimens.

The typical behavior of the panels, as calculated from the finite element analyses, was reasonably ductile up to the failure point. The response was linear up to the cracking of the concrete, and essentially linear with reduced stiffness afterward up to first yielding of the faceplates in the principal tensile direction. Thereafter the load–deformation response assumed a gradually ascending branch until the concrete in the center regions of the panel failed in compression at a shear strain typically around  $5.0\text{--}8.0 \times 10^3$ . The crack pattern and deflected shape of Panel S300NN, at ultimate load, is shown in Fig. 8; it is typical of the damage condition of the panels prior to failure. Thus, the behavior and capacity of the panels was governed by a shear compression failure of the concrete. No buckling of the faceplates was calculated. The calculated damage sequences and failure modes correlated well with the experimentally observed responses.

The axial compression forces applied in some panels was found to result in a slight increase in the yielding and ultimate load capacities, and a slight decrease in ductility. The center partition plate, whether bonded or unbonded, was found to provide no enhancement in the calculated strength or response.

The calculated load–deformation responses for the test panels are compared to the experimentally observed behaviors in Fig. 9. Note that the analysis results shown are the shear strains computed at the center element for each panel; the shear strains varied significantly over the panel areas with the greatest strains occurring near the two inward moving corners. For Panels S315NN and S330NN, Ozaki et al. (2004) did not provide the complete experimental load–deformation responses, but reported only the shear forces and shear strains corresponding to cracking, yielding and ultimate.

In general, the computed responses agreed reasonably well with the experimentally observed behaviors. There was a tendency to

overestimate the cracking loads; earlier cracking in the test panels was likely the result of restrained concrete shrinkage strains which were not considered in the analyses. As well, there was a tendency to underestimate the ultimate load capacity. The strengthened perimeter region and load anchor zones used in the test setup may have had resulted in some unintended strengthening of the panels' load capacity; while an attempt was made to include the strengthened zones in the finite element model, not all details of the connection zones were provided. For the panels with the center partition wall (S300PS and S300PN), the ductility of the post-yield response was significantly underestimated. The partition plate in these specimens was welded to the two faceplates, thus also acting as out-of-plane reinforcement and providing confinement to the core concrete. This out-of-plane confinement, which contributes significantly to increased ductility, was not taken into account in the analyses. Also, with S300PN, the relative slip between the two halves of the specimen, contributing to its apparent ductility, was not adequately captured.

The yield forces and ultimate load capacities calculated for the test panels are compared to the test values in Table 3. The ratio of the calculated to measured yield force had a mean of 1.02 and a coefficient of variation of 12.3%. For the ultimate load capacities, the ratio of calculated to measured values had a mean of 0.96 and a coefficient of variation of 7.2%. In general, the correlations are sufficiently strong given that the strengths were governed by a brittle concrete failure mechanism. The relatively low estimates for the S200 series are somewhat anomalous; it should be noted that Ozaki et al. (2004) also calculated strengths of about 2500 kN for these panels using their analytical procedure. The stronger than expected strengths may be related to panel edge restraint.

#### 4.3. Shear walls

Sasaki et al. (1995) tested seven flanged shear wall specimens under in-plane lateral loading conditions. The specimens varied in height (1250 mm, 1660 mm, and 2500 mm) and web thickness (115 mm, 230 mm, and 345 mm); all web plates were 2.3 mm thick. The flanges, also of SC design, were 830 mm wide and had the same faceplate and overall thickness as the web. The corner columns (i.e., at the intersection of the flanges and the web) had a plate thickness of 4.5 mm, thus producing a heavily confined zone. One specimen had co-acting axial load, and another varied in the nature of the stud anchor pattern used. A sketch of the specimen configuration is given in Fig. 3; additional details are provided by Sasaki et al. (1995).

One particular aspect of the walls that should be noted, critical to their behavior, was the use of 'bending stiffeners'; that is, thick side plates located at the end faces of the flanges. According to Sasaki et al. these 'stiffeners' were provided 'so that shear failure would occur after bending yield of the flange steel plate but prior to bending failure' of the wall. Also, the anchor stud spacing to plate thickness ratio ( $b/t_s$ ), equal to 33, was selected such as to theoretically preclude elastic buckling of the web and flange plates. Thus, these specimens, being relatively complex in the structural mechanisms invoked in their response, represent a stringent test of the analysis procedure.

In the experiments, when subjected to a regime of reversed cyclic lateral displacement, the walls typically exhibited a moderately ductile response governed by yielding and then buckling of the flange and web faceplates. All walls ultimately failed by a compression shear failure of the webs and flanges. As well, all specimens typically exhibited buckling of the web and flange plates, some before the maximum load was reached and some after, despite the fact that the  $b/t_s$  ratio was set to a value that should have prevented buckling.

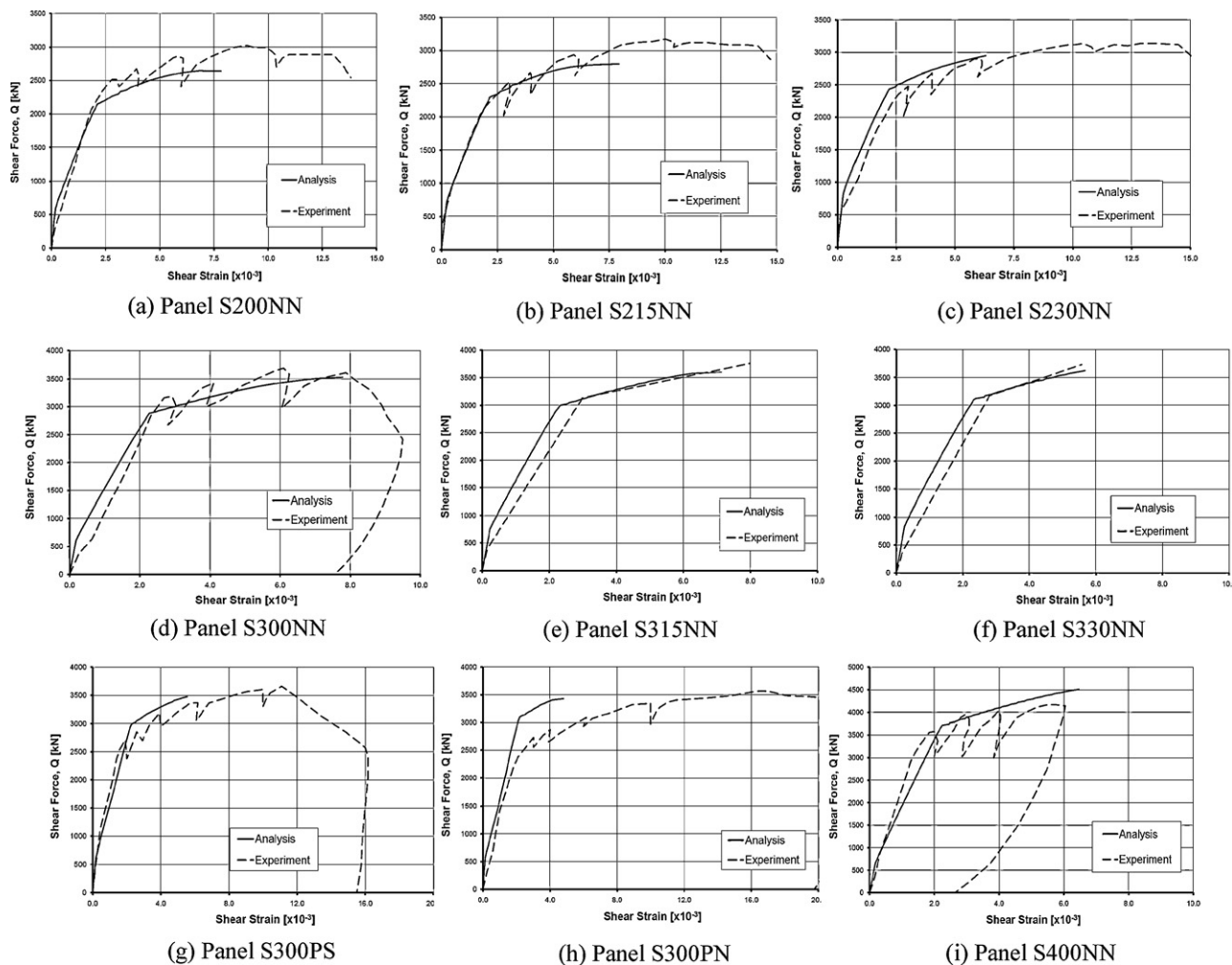


Fig. 9. Shear force–deformation responses for Ozaki shear panels.

The wall specimens were modeled as two-dimensional planar structures; a typical mesh is shown in Fig. 10. The web portions were modeled with the 8 dof rectangular SC element developed earlier. The flanges were also modeled with SC elements, but with the faceplate portion of the element representing the in-plane side plates of the columns. The faceplates of the flanges were modeled using truss bar elements placed on side edges of the flanges. As well, the ‘bending stiffeners’ used on the end faces of the flanges were modeled with truss bar elements; they were not modeled with plate elements to avoid incorrectly invoking lateral confinement to the web. The out-of-plane faceplates of the columns were

represented as smeared out-of-plane reinforcement in the flange elements, thus capturing the significant confinement induced in these zones. Finally, the top and bottom blocks were represented using conventional RC rectangular elements. Only the upper portion of the bottom blocks was modeled, with the bottom edge assumed to be fully fixed along its entire length. One specimen, H10T10N, was not modeled. This specimen differed from H10T10 in that no anchor studs were used to connect the web concrete to the column out-of-plane faceplate. Since the analysis procedure assumes that sufficient anchorage is provided to prevent interfacial slip, the anchorage condition for H10T10N could not be modeled.

Table 3  
Yield and ultimate shear forces of shear panels.

Specimen	Yield force			Ultimate load		
	$Q_{y-exp}$ [kN]	$Q_{y-calc}$ [kN]	$Q_{y-calc}/Q_{y-exp}$	$Q_{u-exp}$ [kN]	$Q_{u-calc}$ [kN]	$Q_{u-calc}/Q_{u-exp}$
S200NN	2290	2112	0.922	2960	2592	0.876
S215NN	2330	2256	0.968	3110	2712	0.872
S230NN	2490	2400	0.964	3110	2808	0.903
S300NN	3070	2808	0.915	3610	3528	0.977
S315NN	3130	3000	0.958	3760	3600	0.957
S330NN	3170	3096	0.977	3730	3624	0.972
S300PS	2680	3000	1.119	3580	3480	0.972
S300PN	2350	3072	1.307	3510	3432	0.978
S400NN	3510	3720	1.060	4100	4512	1.100
Mean			1.021			0.956
COV (%)			12.3			7.2

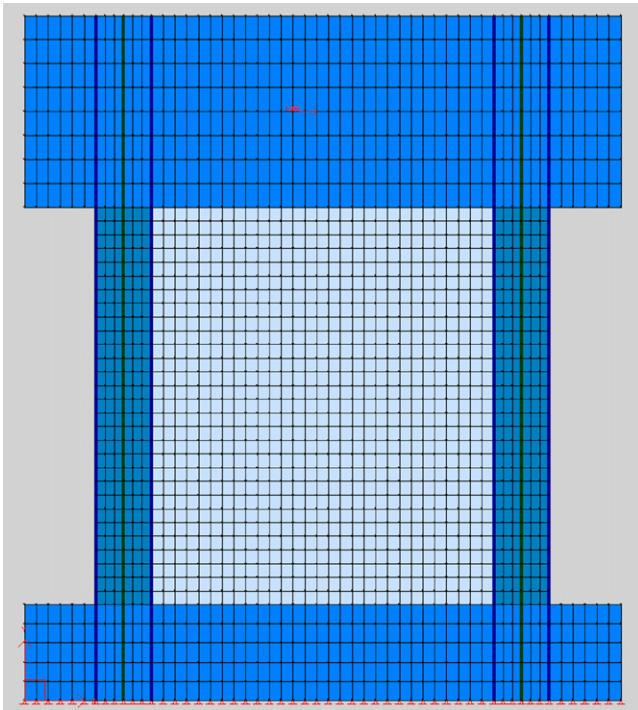


Fig. 10. Finite element model for Sasaki wall specimen H10T10.

The material properties used for the analyses were as described by Sasaki et al. (1995). The yield and ultimate strengths of the 2.3 mm web/flange faceplate steel were taken as 286 MPa and 420 MPa, respectively; for the 4.5 mm column faceplate steel, the yield and ultimate strengths were 294 MPa and 438 MPa, respectively. The strain hardening and ultimate strain characteristics were not provided; thus, a tri-linear response was assumed with strain hardening at  $20 \times 10^3$  and fracture at  $180 \times 10^3$  (i.e., a highly ductile response). Also, neither the thickness nor the material properties of the ‘bending stiffener’ plates was provided; the plates were thus assumed to be 25 mm thick (as scaled from the sketch provided), with steel properties similar to that of the column faceplate steel. The concrete used in Specimens H10T10, H10T10V, and H15T10 had a compressive strength of 32.7 MPa and an initial modulus of elasticity of 23,400 MPa. For Specimens H07T10, H10T05 and

H10T15, the concrete possessed a compressive strength of 29.7 MPa and a modulus of elasticity of 20,700 MPa.

Lateral load was applied as an imposed displacement at the mid-height of the top block. The loading regime consisted of a reversed cyclic displacement protocol: one cycle at each amplitude level with the amplitude increasing by 2 mm successively. A displacement step size of 0.5 mm was used for Specimens H10T10, H10T10V, H10T05 and H10T15. Step sizes of 0.25 mm and 1.0 mm were employed with Specimens H07T10 and H15T10, respectively. Typically, the maximum load capacity was reached during the excursion to 10 mm, thus the loading was arbitrarily terminated after the 14 mm displacement cycle, except for Wall H15T10 (a taller wall) which was taken to 24 mm displacement. A constant axial load of 2520 kN (nominally 3.0 MPa) was co-applied with the lateral displacement regime for Specimen H10T10V.

The analyses found all walls to be shear-critical, governed by failure of the web concrete in vertical planes adjacent to the flanges, in horizontal planes near the base, and in diagonal planes across the center of the web. In most cases, the damage was concentrated in the compression toe regions of the web. For some walls, concrete crushing at the base of the flanges was also found. Shown in Fig. 11, for example, are the deflection and damage states of Specimen H10T10. These findings agreed well with the damage patterns reported by Sasaki et al. (1995).

The analyses also found that although web plate buckling occurred relatively early in the response histories, the buckling was localized in the compression toe regions of the walls. No faceplate buckling was found to occur in the flanges. The experimental observations, on the other hand, indicated widespread buckling of the web and flange plates. Thus, the analyses did not correspond well with the test results in this respect. This is a direct consequence of the modified Euler buckling expression, as suggested by Usami et al. (1995) and implemented in this work, being inadequate in properly representing buckling behavior in SC structures.

The ultimate load capacities calculated for the walls correlated exceptionally well with the experimental values. As summarized in Table 4, the ratio of the calculated to measured wall strengths had a mean of 0.99 and a coefficient of variation of 7.6%. This level of accuracy, especially for shear-critical structures, is well within the bounds that one should reasonably expect for reinforced concrete structures.

The computed load–deformation responses also, in general, correlated well with the experimental responses as seen in Fig. 12. [Note that the experimental responses plotted in Fig. 12 repre-

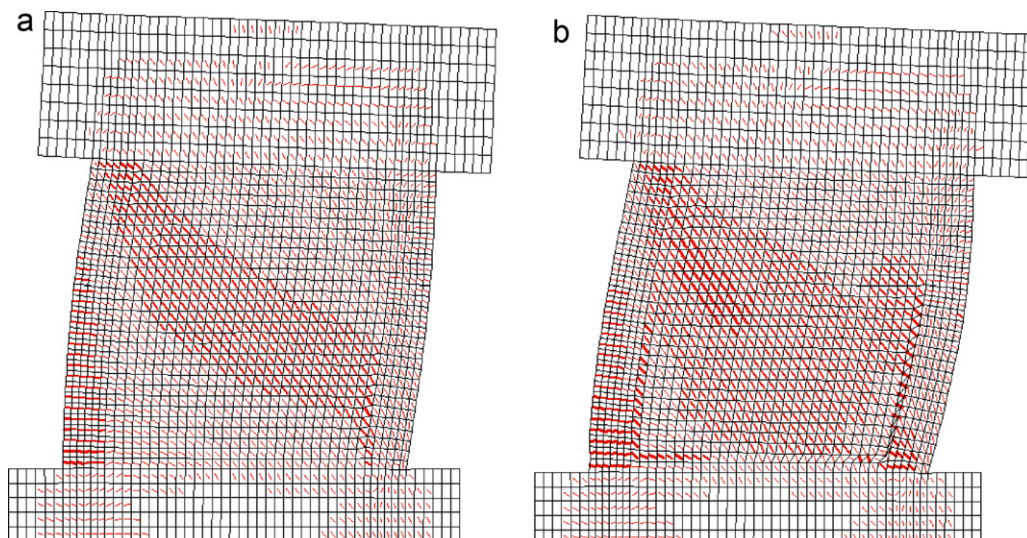
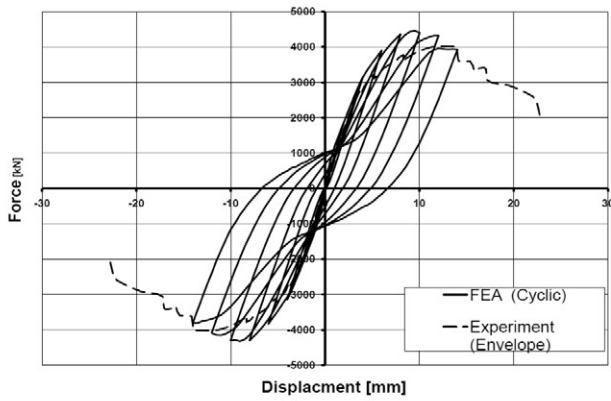


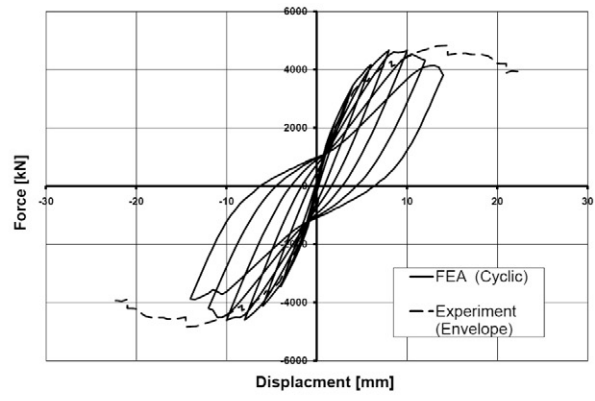
Fig. 11. Calculated crack pattern and deflected shape [20 $\times$ ] for H10T10. (a) At ultimate load. (b) At 14 mm displacement.

**Table 4**  
Specimen load capacities.

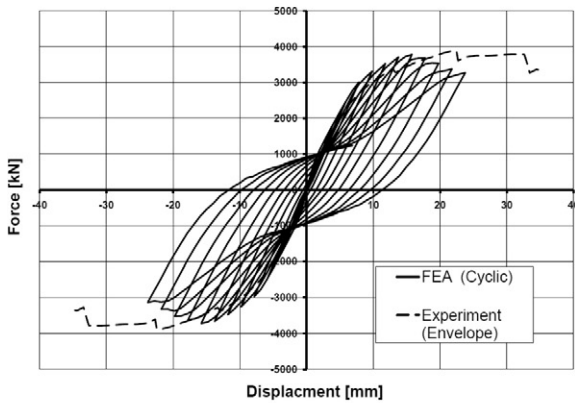
Specimen	Experiment			Analysis			$Q_{cal}/Q_{exp}$
	$\tau_u$ [MPa]	$A_e$ [mm <sup>2</sup> ]	$Q_{exp}$ [kN]	$Q_{cal-POS}$ [kN]	$Q_{cal-NEG}$ [kN]	$Q_{cal-AVG}$ [kN]	
H10T10	9.4	434,700	4090	4461	4322	4392	1.074
H10T10V	11.3	434,700	4910	4665	4611	4638	0.945
H15T10	9.5	434,700	4130	3780	3722	3751	0.908
H07T10	10.6	434,700	4610	4847	4734	4791	1.039
H10T05	12.6	204,125	2570	2764	2721	2742	1.067
H10T15	9.5	691,725	6570	6101	6017	6069	0.922
						Mean	0.993
						COV (%)	7.61



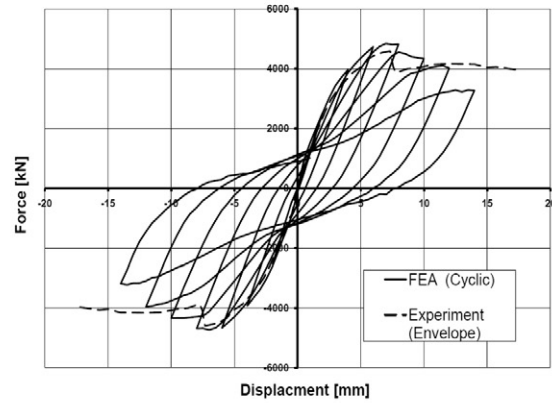
(a) Wall H10T10



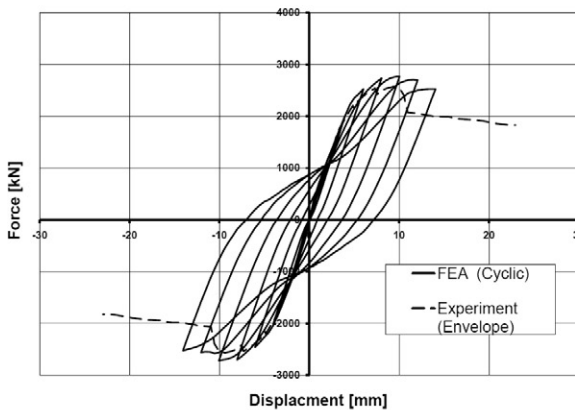
(b) Wall H10T10V



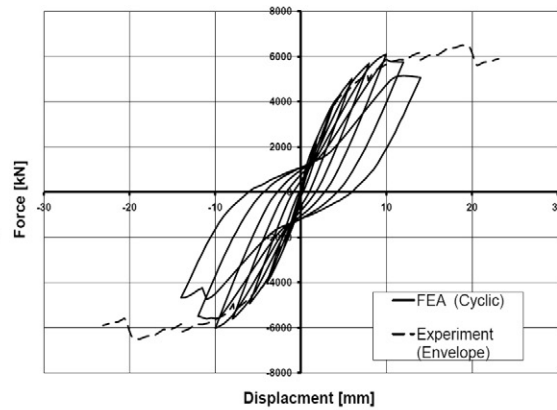
(c) Wall H15T10



(d) Wall H07T10



(e) Wall H10T05



(f) Wall H10T15

Fig. 12. Load-deflection responses of Sasaki shear walls.

sent the envelopes of the hysteresis curves. The negative envelopes shown are the mirror images of the positive envelopes since the responses for the negative displacement half cycles were not reported.] The initial stiffnesses of the walls, the displacements at ultimate load, and the trend of the post-peak decay in strength were captured accurately. The general tendency, however, was to overestimate strength and stiffness in the latter stages of the pre-peak responses. This may be a consequence of several factors, the most significant being that: (i) buckling of the faceplates was not well represented; (ii) no attempt was made to account for interfacial slip between the faceplates and the concrete; and (iii) two-dimensional modeling, in which the thickness (and thus stiffness) of the flanges is collapsed into the plane of the web, over-estimates the lateral confinement of the webs. In addition, no attempt was made to consider tensile failure of the stud anchors, which was observed to occur in some tests. Nevertheless, the computed responses provided an accurate estimate of the strength and ductility of the walls.

## 5. Summary and conclusions

The Disturbed Stress Field Model (DSFM) is a smeared rotating crack model for reinforced concrete previously developed as a refinement of the Modified Compression Field Theory (MCFT) and proven successful in providing accurate simulations of the behavior of reinforced concrete (RC) structures. In this study, the DSFM was further developed to enable the analysis of steel-concrete (SC) composite panel elements. The enhanced formulation was implemented into an existing nonlinear finite element analysis (FEA) algorithm for the analysis of two-dimensional planar structures (VecTor2). Verification studies were then undertaken, modeling the response of various SC test specimens including panels subjected to uniaxial compression, panels subjected to in-plane shear, and shear walls subjected to reversed cyclic lateral displacements.

Conclusions that can be drawn from this work include the following:

1. The smeared rotating crack approach, based on the DSFM, is viable basis for the formulation of a computational model for SC planar elements.
2. The SC element developed accordingly can be successfully integrated into a nonlinear finite element analysis algorithm. The resulting FEA implementation is numerically stable and robust, and computationally efficient, even under conditions of reversed cyclic loading and post-peak response.
3. The smeared element approach represents an advancement over commonly used FEA methods for analysis of SC structures, which typically rely on three-dimensional micro-modeling of wall details and thus entail significantly more modeling and computational effort.
4. In modeling the behavior of test specimens subjected to various in-plane loading conditions, the SC formulation developed is able to provide accurate predictions of ultimate strength. The ratio of the calculated to measured strength for the 19 specimens examined had a mean of 0.99 and a coefficient of variation of 7.1%.
5. The formulation also provides accurate simulations of pre- and post-peak load-deformation response, chronology of damage and failure mode. In particular, it correctly captures the lack of post-peak ductility in some shear-critical structures without the use of artificial limits placed on strains or other parameters.
6. Strong correlations between calculated and experimental results can be obtained using basic finite element modeling techniques, basic (default) options for all analysis parameters and material models, and without the use of complex elements such as link or bond elements. No fine tuning of analysis parameters or structure modeling is required.
7. Buckling of steel faceplates was integrated into the formulation by implementing the basic Euler buckling equation for plates. However, the Euler expression does not produce results consistent with the buckling of web and flange faceplates observed in several test programs.
8. The analysis model tends to typically overestimate structural stiffness in the latter stages of pre-peak response. This may be a result of the interfacial slip between the faceplates and the concrete not being considered; the analysis model assumes that sufficient anchorage is provided between the faceplates and the concrete to allow the structure to act monolithically. This assumption does not, however, seem to have an adverse affect on predicted strengths.
9. The rupture of steel anchor studs, noted in some test programs, is not captured. Again, the model assumes sufficient anchorage has been provided.
10. Given a lack of suitable relevant information in the literature, conservative assumptions are made in the model regarding average crack spacing and tension stiffening effects in SC elements. Both are important mechanisms that figure prominently in calculating the response of shear-critical elements and, thus, warrant further investigation.

Finally, it should be noted the analyses support experimental observations that shear-critical SC elements generally behave as well or better than comparable RC elements. However, post-peak ductility may be limited in some cases even though element strength may be governed by yielding of the faceplates in tension. As the faceplates yield in the principal tension direction, they simultaneously lose strength in the principal compression direction (according to most yield criteria), shedding load to the concrete. If the concrete is extensively cracked, then the additional tensile straining coupled with compression softening effects may result in the concrete simultaneously losing compression load capacity at stresses well below the nominal compressive strength of the concrete and with reduced ductility.

## Acknowledgments

This work was sponsored by the U.S. Nuclear Regulatory Commission through Contract NRC DR 04 10 139. The project officer for this contract was Dr. Jose Pires. The support received from the U.S. Nuclear Regulatory Commission was greatly appreciated. The findings and opinions expressed in this paper are those of the authors, and do not necessarily reflect the views of the U.S. Nuclear Regulatory Commission.

## References

- CEB FIP, 1990. Model Code for Concrete Structures, Design Code, Comité EURO International du Béton, 437 pp.
- CSA A23.3, 2004. Design of Concrete Structures. Canadian Standards Association, Mississauga, Ontario, Canada, 214 pp.
- Dhakal, R.P., Maekawa, K., 2002. Path-dependent cyclic stress-strain relationship of reinforcing bar including buckling. *Engineering Structures* 24 (11), 1383–1396.
- Driver, R.G., Kulak, G.L., Kennedy, D.J.L., Elwi, A.E., 1998. Cyclic tests of four story steel plate shear wall. *ASCE Journal of Structural Engineering* 124 (2), 112–120.
- Eom, T.S., et al., 2009. Behavior of double skin composite wall subjected to in-plane cyclic loading. *ASCE Journal of Structural Engineering* 135 (10), 1239–1249.
- Hajjar, J.F., 2002. Composite steel and concrete structural systems for seismic engineering. *Journal of Constructional Steel Research* 58, 703–723.
- Liang, Q., et al., 2004. Local buckling of steel plates in double skin composite panel under biaxial compression and shear. *ASCE Journal of Structural Engineering* 130 (3), 443–451.
- Ozaki, M. et al., 2001. Study on steel plate reinforced concrete bearing wall for nuclear power plants (Part 1 2). SMiRT16, August, 2001.
- Ozaki, M., et al., 2004. Study on steel plate reinforced concrete panels subjected to cyclic in-plane shear. *Nuclear Engineering and Design* 228 (13), 225–244.

- Palermo, D., Vecchio, F.J., 2003. Compression field modelling of reinforced concrete subjected to reversed loading: formulation. *American Concrete Institute Structural Journal* 100 (5), 616–625.
- Sasaki, N. et al., 1995. Study on a concrete filled steel structure for nuclear power plants part 3: shear and bending loading tests on wall member, SMiRT13, Porto Alegre, Brazil, August 1995, pp. 27–32.
- Suzuki, N. et al., 1995. Study on a concrete filled steel structure for nuclear power plants part 4: analytical method to estimate shear strength, SMiRT13, Porto Alegre, Brazil, August 1995, pp. 33–38.
- Takeda, T. et al., 1995. Experimental study on shear characteristics of concrete filled steel plate wall. SMiRT13, Porto Alegre, Brazil, August 1995, pp. 3–14.
- Takeuchi, M. et al., 1995. Study on a concrete filled structure for nuclear power plants (part 1 4) SMiRT13, Porto Alegre, Brazil, August 1995, pp. 15–20.
- Usami, S. et al., 1995. Study on a concrete filled steel structure for nuclear power plants part 2: compressive tests on wall members, SMiRT 13, Porto Alegre, Brazil, August, 1995, pp. 21–26.
- Vecchio, F.J., 1989. Nonlinear finite element analysis of reinforced concrete membranes. *ACI Structural Journal* 86 (1), 26–35.
- Vecchio, F.J., 1990. Reinforced concrete membrane element formulations. *ASCE Journal of Structural Engineering* 116 (3), 730–750.
- Vecchio, F.J., 1992. Finite element modelling of concrete expansion and confinement. *ASCE Journal of Structural Engineering* 118 (9), 46–56.
- Vecchio, F.J., 1999. Towards cyclic load modelling of reinforced concrete. *American Concrete Institute Structural Journal* 96 (2), 193–202.
- Vecchio, F.J., 2000. Disturbed stress field model for reinforced concrete: formulation. *ASCE Journal of Structural Engineering* 126 (9), 1070–1077.
- Vecchio, F.J., 2001. Disturbed stress field model for reinforced concrete: implementation. *ASCE Journal of Structural Engineering* 127 (1), 12–20.
- Vecchio, F.J., Collins, M.P., 1986. The modified compression field theory for reinforced concrete elements subjected to shear. *Journal of the American Concrete Institute* 83 (2), 219–231.
- Vecchio, F.J., et al., 1996. Nonlinear analysis of reinforced concrete; the University of Toronto experience. In: *Proc. Third Asian Pacific Conference on Computational Mechanics*, Seoul, Korea.
- Wright, H.D., et al., 1991. The experimental behavior of double skin composite elements. *Journal of Constructional Steel Research* 19 (2), 97–110.
- Zhou, J. et al., 2010. Seismic Performance of Composite Steel Plate Reinforced Concrete Shear Wall, *ASCE Conf. Earth and Space 2010: Engineering, Science, Construction, and Operations in Challenging Environments*, pp. 3002–3010.